IEEE Access
Multidisciplinary | Rapid Review | Open Access Journal

IEEE RELIABILITY SOCIETY SECTION

Received March 26, 2021, accepted May 22, 2021, date of publication May 26, 2021, date of current version June 3, 2021.

Digital Object Identifier 10.1109/ACCESS.2021.3083793

Reliability of a Power System With High Penetration of Renewables: A Scenario-Based Study

YING-YI HONG[1], (Senior Member, IEEE), CHIN-I WU[1], TZU-HSUN HSIAO[2], AND CHANG-SHIEN LIN[2]

[1]Department of Electrical Engineering, Chung Yuan Christian University, Taoyuan 32023, Taiwan
[2]Institute of Nuclear Energy Research, Taoyuan 32546, Taiwan

Corresponding author: Ying-Yi Hong (yyhong@ee.cycu.edu.tw)

This work was supported in part by the Institute of Nuclear Energy Research, Taiwan, under Grant 108-B-015 and Grant NL1100131, and in part by the Ministry of Science and Technology, Taiwan, under Grant MOST 109-2221-E-033-011.

ABSTRACT Reliability is a crucial consideration in the expansion of generation or transmission in a bulk power system, especially in a power grid with a high penetration of renewables. Reliability indices, such as loss of load probability (LOLP), are generally evaluated to determine the adequacy of a bulk power system in the future. When a Monte-Carlo simulation is conducted to evaluate the LOLP, the computational time is long because chronological time-series data are involved. This work proposes a novel scenario-based method for studying the LOLP in a bulk power system with a high penetration of renewables. Scenarios are generated by aggregating Markov states of hourly loads, photovoltaic power generations and wind power generations. The power flow result in each scenario is examined to ensure power balance among demand, supply and losses, so the LOLP can be obtained. This novel scenario-based method is more efficient than the traditional chronological time-series approach because the number of considered scenarios is much smaller than the number of considered time-series cases. A set of realistic data regarding Taiwan power system, consisting of 2078 buses associated with a peak load of 39.178 GW, wind power of 6.938GW and photovoltaic power of 20 GW in 2025 is used to validate the proposed method.

INDEX TERMS Loss of load probability, Markov model, Monte-Carlo simulation, renewables, reliability.

I. INTRODUCTION

The operation and planning of electric power grids is becoming increasingly complex on account of the high penetration of renewables and the transactions of power market [1]. Reliability studies are generally performed in the planning or short-term scheduling stages. Power system reliability indicates the overall ability of the power system to deliver its power generation to end-users [2]–[5]. Typical power system reliability studies are categorized into two groups – those that address adequacy and those that address security [6]. Adequacy is a static condition and is determined by whether sufficient facilities are available to satisfy demand. Security, which relates to dynamic phenomena of the system, refers to the ability of the system to respond to disturbances. Most reliability studies address adequacy. Detailed static and dynamic aspects of bulk power system reliability evaluations can be found elsewhere [7].

One of the most popular indices of reliability in a bulk power system is the loss of load probability (LOLP) [8]. Rashidaee *et al.* formulated an LOLP-constrained generation expansion planning problem as a mixed integer nonlinear programming problem [9]. Choi *et al.* proposed a methodology that used a probabilistic reliability criterion to determine an optimum plan for transmission system expansion, minimizing the expected cost by considering the LOLP constraint [10]. Xu and Zhuan presented a probabilistic method to assess the system LOLP and to estimate the spinning reserve, which depends on the uncertainty of wind power generation and the forecasted load demand [11]. Deulka *et al.* presented a Markov-modulated fluid queue to model the LOLP that is associated with a battery energy storage system (BESS), which serves an uncertain demand and copes with intermittent renewable power generation [12].

The associate editor coordinating the review of this manuscript and approving it for publication was Jian Guo.

The analytical enumeration method (AEM) and Monte Carlo simulation (MCS) are commonly used to evaluate system states for reliability evaluation [13]. The AEM analyzes all possible system states to obtain accurate results, resulting in high computational complexity for a large-scale power system. MCS, in contrast, provides information about a bulk power system by randomly sampling system data in a manageable set. Xie *et al.* presented a uniform-design technique to generate the system states, yielding sampled states that were more uniform and representative in the whole state space than were the enumerated system states in the AEM or the randomly generated system states in MCS [13]. Peng *et al.* presented a method to partition the chronological system state sequence produced by a sequential MCS into a set of mutually exclusive events for a composite generation and transmission system [14].

Reliability studies that involve the LOLP were also concerned in microgrids [15]–[18] and standalone (off-grid) power systems [19]–[22]. MCS was conducted to study storage-reserve sizing [15]. A time-varying probability-ordered tree was presented to evaluate the LOLP in [16]. A model of load shedding minimization combined with sequential MCS was used to study energy storage sizing in [17]. An energy storage size was determined for a specific LOLP in a microgrid with a large penetration of renewables, considering generation and load forecast error in [18]. A stand-alone hybrid generation system capacity was determined from the cost and the LOLP considering PV and wind power in [19]. Markov model and frequency-duration reliability techniques were used to evaluate reliability indices for a stand-alone hybrid photovoltaic (PV)-BESS system in [20]. Markov models were used to simulate the stochastic behavior of a microgrid and to obtain a realistic value of the LOLP, taking the failure and repair rates of each component into account in [21]. Reliability and emissions were estimated for a hybrid PV-BESS system and compared with those for a system with diesel generators in [22].

According to the above discussions, the aforementioned works have at least one limitation as follows:

(1) Power flow in the power grid is ignored [8]–[12], [15]–[22]; only whether the power generation and transmission capacities suffice for the demand is determined. For a large bulk composite power system with many large power plants and renewables farms, a comprehensive power flow study considering spinning reserve is essential.
(2) MCS is widely used to carry out reliability studies. A chronological time-series approach takes a long computational time [15], [17].
(3) Implementing MCS with time-coupling constraints is difficult, such as when the energy and power of a BESS are related [13], [14].

To overcome the above limitations, this paper proposes a novel scenario-based method for exploring the LOLP in a bulk power system with a high penetration of renewables. The Taiwan power system in 2025 will be used as an example. The contributions of this paper can be summarized as follows.

(1) Not only the power balance between power generation and demand is confirmed but also the violation of spinning reserves from generators is examined in all scenarios by performing power flow studies. This additional but essential factor (spinning reserves) was generally ignored in previous studies.
(2) The fuzzy-c-means algorithm is utilized to develop the Markov models of load, wind power and photovoltaic power in the individual state spaces, which are further transformed into an aggregated scenario space.
(3) Rather than solving the LOLP problem in a chronology space, the proposed method deals with the LOLP in a scenario space, significantly reducing the computational time that is required by MCS.
(4) The time-coupling constraint is converted into the scenario-coupling constraint in the LOLP problem using a fixed probability transition matrix, which is proved to be convergent using realistic Taiwan power system data.

The rest of this paper is organized as follows. Section II describes the relevant Markov theory. Section III presents the proposed method. Section IV discusses simulation results. Section V draws conclusions and suggests directions for future work.

II. BACKGROUND OF MARKOV MODEL

Solving this reliability problem is prohibitively time-consuming owing to the extremely large number of chronological parameters and constraints that are involved. For example, if 8760 hourly power flows are studied to obtain the LOLP, then 8760 sets of bus data and line data must be prepared. Among all relevant parameters, the hourly loads, photovoltaic power and wind power are essential [23]–[26]. This paper converts this chronological problem into a scenario-based problem, in which the probabilities and durations of load, wind power and PV power states can be obtained by applying Markov theory. Specifically, rather than using a traditional chronological time series with increasing hours from h $=$ 1 to h $=$ 8760 in sequence, the conditions of the power system are varied among Markovian scenarios (Markov chain) according to system transition rates (probabilities).

The Markov model captures the probability, duration and frequency of a state in a stochastic process [27], [28]. Suppose that a component (such as photovoltaic power, P_{PV}) has M states, m $=$ 1, 2, …, M. The transition rates between any two states are λ and μ. Let P_m be the probability associated with the m*th* state. Then

$$\sum_{m=1}^{M} P_m = 1 \tag{1}$$

$$[T_s]\,[P_1 \ldots P_m \ldots P_M]^t = 0 \tag{2}$$

where $[T_s]$ is the state transition matrix. For example, Fig. 1 displays a three-state Markov model. The state

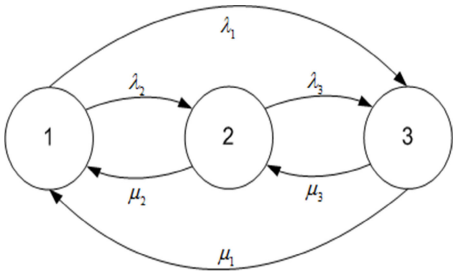

FIGURE 1. Three-state Markov model.

transition matrix can be defined as (3).

$$[Ts] = \begin{bmatrix} -(\lambda_1+\lambda_2) & \mu_2 & \mu_1 \\ \lambda_2 & -(\mu_2+\lambda_3) & \mu_3 \\ \lambda_1 & \lambda_3 & -(\mu_1+\mu_3) \end{bmatrix} \quad (3)$$

To evaluate λ and μ, the transitions from a state to any other state in a given time-series, which consists of these three states, must be counted. Suppose that the number of state transitions is given, as shown in Table 1.

TABLE 1. Number of transitions among states.

From state / To state	State 1	State 2	State 3
State 1	6	1	1
State 2	2	7	1
State 3	2	2	8
total	10	10	10

From Table 1, the transition probability matrix $[Tp]$ can be calculated using (4).

$$[Tp] = \begin{bmatrix} 6/10 & 1/10 & 1/10 \\ 2/10 & 7/10 & 1/10 \\ 2/10 & 2/10 & 8/10 \end{bmatrix} \quad (4)$$

The state transition matrix $[Ts]$ is defined by (5) where the upper triangle of the M × M matrix $[Ts]$ is composed of μ's between pairs of states and the lower triangle consists of λ's between pairs of states. Each diagonal term of $[Ts]$ equals the negative sum of all off-diagonal terms in the same column.

$$[Ts] = \begin{bmatrix} -4/10 & 1/10 & 1/10 \\ 2/10 & -3/10 & 1/10 \\ 2/10 & 2/10 & -2/10 \end{bmatrix} \quad (5)$$

According to (3) and (5), $\lambda_1 = \lambda_2 = \lambda_3 = 2/10$, $\mu_1 = \mu_3 = \mu_2 = 1/10$. The absolute value of the diagonal term for state m in (5) is defined as the *rate of departure* of state m. The duration of a state equals the reciprocal of its rate of departure [28]. Solving (1) and (2) leads to three probabilities: 0.2, 0.3 and 0.5.

Appendix A provides the convergence theorem for a Markov chain [29]. This theorem is useful when a scenario-coupling constraint is involved. This scenario-coupling constraint corresponds to the time-coupling relation between the energies of BESS at times h and (h + 1).

III. PROPOSED METHOD

A. FUZZY-C-MEANS (FCM)

Given a time series, the corresponding Markov states can be obtained using a fuzzy-c-means (FCM) algorithm [30]. In this paper, 8760 historic wind speeds and irradiances from 2018 serve as references for 2025. Assume that the profile of 8760 hourly loads in per unit in 2025 is the same as that in 2018. The operational states of system load, PV power generation and wind power generation are discretized to $P_d(s_1)$, $P_{pv}(s_2)$ and $P_w(s_3)$, respectively, where s_1, s_2 and s_3 are the state indices.

Each dataset of load, PV power and wind power has some fuzzy membership values $\mu_{c\zeta}$, associated with a cluster in the FCM algorithm. $\mu_{c\zeta}$ signifies the membership value that relates V_c to X_ζ where X_ζ is the ζ-th known dataset and V_c is the unknown central vector of the c-th cluster. The membership value is obtained by minimizing an objective function [30]:

$$J(\mu_c, V_c) = \sum_{\zeta=1}^{N} \sum_{c=1}^{C} \mu_{c\zeta}^{\rho} \left\| X_\zeta - V_c \right\|^2, \quad 1 \le \rho \le \infty \quad (6)$$

where N is the known number of datasets and C is a given number of clusters. When the FCM converges, the N datasets are grouped into C clusters.

In this paper, the numbers of clusters (C) for $P_d(s_1)$, $P_{pv}(s_2)$ and $P_w(s_3)$ are 15, 8 and 13, respectively. Specifically, the system loads in 8760 hours are discretized with intervals of approximately 1000 MW between the peak 39178 MW and the off-peak 17734 MW. The number of clusters for irradiances is estimated around every 100W/m^2 from 300W/m^2 to 1000W/m^2. The wind power data are clustered about every 1m/s within the range between the cut-in speed and the rated speed. The center V_c of cluster c corresponds to the representative vector of a cluster and is regarded as a state in the Markov model. The dimensions of X_ζ and V_c are 1 × 1 and $N = 8760$.

B. AGGREGATION OF $P_d(s_1)$, $P_{pv}(s_2)$ AND $P_w(s_3)$

After the individual Markov states of $P_d(s_1)$, $P_{pv}(s_2)$ and $P_w(s_3)$ have been identified, these Markov states can be aggregated to generate the probabilities and durations of all scenarios. Suppose that $s_1 = 1, 2, \ldots, C1$; $s_2 = 1, 2, \ldots, C2$; $s_3 = 1, 2, \ldots, C3$. In total, C1 × C2 × C3 (that's, 15 × 8 × 1560 = C, s = 1, 2, . . . , C) scenarios need to be explored. The probability and duration of a scenario can be calculated as follows.

(i) The product of the probabilities of any 3 states ($P_d(s_1)$, $P_{pv}(s_2)$ and $P_w(s_3)$) yields the probability of a scenario.

(ii) The rate of departure of a scenario is the sum of the rates of departure of any 3 states ($P_d(s_1)$, $P_{pv}(s_2)$ and $P_w(s_3)$). The reciprocal of the rate of departure for this scenario is its duration (d (s)).

C. DATA PREPARATION

Data regarding the Taiwan power system in 2025 were used to show the applicability of the proposed method in this paper. The system comprises 2078 buses, 47 combined cycle units, 19 hydro units, 10 pumped storage units, and 24 coal-fired units. The summer peak load and winter off-peak load in 2025 are estimated to be 39.178 and 17.734 GW, respectively. A total of 8760 hourly loads in 2025 are generated from the historical load profile in 2018.

The photovoltaic power of 20GW is allocated to 168 buses each of which has a load of around 110∼120 MW. The 8760 hourly photovoltaic powers at each bus were generated from HOMER software using NASA weather data [31]. Since more than 50% of photovoltaics in Taiwan are installed in its central area, the Markov states of the photovoltaics in the northern and southern areas are assumed to be the same as those in the central area except for the capacity.

Onshore wind farms with a total of wind power capacity of 1.2 GW were installed at 104 buses of 69 kV on the west coast. Each bus has several wind turbines with total capacities of 11-12 MW. Offshore wind farms with a total capacity of 5.738 GW will be installed in 2025. Six 161 kV and two 345 kV buses are identified to connect the offshore wind farms to provide a total capacity of 5.738 GW. The historical wind speeds at a height of 10 m in both onshore and offshore wind farms were input to HOMER software [31] to generate 8760 hourly wind power generations at heights of 122m and 135m, respectively. The Markov states of wind power in the onshore wind farms, with the exception of the wind power capacity, are assumed to be the same as those in the offshore farms.

Since a comprehensive power flow study using PSS/E software [32] will be performed in the MCS, different power generations from generators shall be set. Let "Net Load(s) = System_Load(s) - total_PV(s) - total_WT(s)" where System_Load(s), total_PV(s), and total_WT(s) are system load, total PV power and total wind power in scenario s, respectively. Five sets of on-line generators were implemented according to the following net load(s): (a) net load(s) > 3.6 GW, (b) 3.6 GW ≥ net load(s) >3.2 GW, (c) 3.2 GW ≥ net load(s) > 2.8 GW, (d) 2.8 GW ≥ net load(s) > 2.4 GW, and (e) 2.4 GW ≥ net load(s). These 5 sets of on-line generators ensure that no wind or photovoltaic power will be curtailed and no line congestion will occur.

Because all combined cycle units in this power system with a high penetration of renewables are designed to provide spinning reserves, all combined cycle units are set as swing buses. When the power flow algorithm is not convergent or the MW limit of one of the combined cycle units is violated, this scenario is considered to be one in which the power supply is inadequate to meet the system demand.

D. BESS MODEL AND CONVERGENCE THEOREM OF MARKOV CHAIN

The BESS will be also used in the Taiwan power system in 2025. The operation of a BESS must meet the following constraints, which are generally not considered in traditional power flow studies, because the traditional power flow problem does not involve inequality constraints or the time-coupling constraint.

$$E_b^{min} \le E_b(s) \le E_b^{Max} \tag{7}$$

$$0 \le P_b^{dis}(s) \le P_b^r \tag{8}$$

$$0 \le P_b^{ch}(s) \le P_b^r \tag{9}$$

$$E_b(s') = E_b(s) + \eta_c \times P_b^{ch} \times d(s) - \eta_d \times P_b^{dis} \times d(s) \tag{10}$$

where E_b^{min}, $E_b(s)$ and E_b^{Max} are the minimum energy, energy in the present scenario s, and the maximum energy (10MWh) of BESS, respectively, at a specified bus. $P_b^{dis}(s)$ and $P_b^{ch}(s)$ are the discharging and charging powers at a specific bus in scenario s. The rated power P_b^r is 10 MW. The term $d(s)$ is the duration of scenario s and η_c (η_d) denotes the charging (discharging) efficiency (85% (100%) herein). The strategy for charging and discharging the BESS is based on power generation from photovoltaic farms. If total power generation from photovoltaic farms exceeds 500 MW, then the charging mode is activated; otherwise, the discharging mode is activated. The total MW in the Taiwan power system in 2025 is 590 MW, allocated at various 59 buses.

The symbol s′ in (10) denotes the scenario after scenario s. Scenario s′ is randomly generated and identified using cumulative probability. For example, the probabilities of transitions from scenario 1 to scenario 1, scenario 2 and scenario 3 are 6/10, 2/10, and 2/10, respectively, in (4). Let MCS iteration index IT = 1 and Markov chain index k = 1. Generate a random number $\gamma 0$ uniformly within [0,1]. If $\gamma 0 \le 0.6$, then scenario 1 does not change. If $0.6 < \gamma 0 \le 0.8$, then the next scenario will be scenario 2. If $0.8 < \gamma 0 \le 1.0$, then the next scenario will be scenario 3. Increase k by 1. Compute $[Tp]^k$ and repeat the above process until convergence ($[Tp]^k$ becomes nearly fixed) as described in Appendix A. When a fixed $[Tp]$ is obtained in the first MCS iteration, the diagonal terms of $[Tp]$ represent the probabilities of all scenarios. In the subsequent MCS iterations, a random number $\gamma 0$ is generated to determine the next scenario using the cumulative probability from the fixed $[Tp]$ until the probability of each scenario is close to its corresponding diagonal term of $[Tp]$.

E. MONTE-CARLO SIMULATION

The LOLP of a power system relies on the Forced Outage Rates (FOR) of different types of generators. In this paper, the FORs of combined cycle units, hydro units including pumped storage units, coal-fired units, photovoltaics and wind turbines are 0.0414, 0.0468, 0.0516, 0.0500 and 0.0500, respectively. The maximum number of Monte-Carlo simulations is set at 10000. The MCS steps were developed using PSS/E power flow software [32] to study the reliability of the Taiwan power system considering spinning reserves as follows.

Step 1: Let IT, td and TD be the MCS index, the total duration for which the power generation is inadequate to meet the system demand, and the total duration of all scenarios in MCS, respectively. Also, let g and s be the generator index ($g = 1, 2, \ldots, G$; $G = 100$ traditional generators plus 168 photovoltaic buses and 112 buses with wind turbines herein; in total $G = 380$) and the scenario index ($s = 1, 2, \ldots, C$; $C = 1560$ herein), respectively. Let PG(g,s) be the power generation of the g-th unit in scenario s. Initially, $s = 1$, $td = 0$ and $TD = 0$. Let the Markov chain index $k = 1$.

Step 2: $TD = TD + d(s)$.

Step 3: Use "Net Load(s)" to set the generator buses and their scheduled power generations, as described in Sec. III.C.

Step 4: Let $g = 1$.

Step 5: Generate a random number $\gamma 1$ uniformly within [0,1].

Step 6: If $\gamma 1 <$ FOR(g), then PG(g,s) = 0 MW; otherwise, PG(g,s) = scheduled value. $g = g + 1$.

Step 7: If $g > G$, then go to Step 8; otherwise, go to Step 5.

Step 8: Run the PSS/E power flow software package.

Step 9: If the power flow algorithm is not convergent or the MW limit of one of the combined cycle units is violated, then this scenario is considered to be one in which the power supply cannot meet the system demand. $td = td + d(s)$.

Step 10: Generate a random number $\gamma 2$ uniformly within [0,1].

Step 11: Identify the interval, in which $\gamma 2$ is located, of the cumulative probability for scenario s to determine the next scenario s'. (See Sec. III.D)

Step 12: If $IT = 1$, then $k = k + 1$ and compute $[Tp]^k$; otherwise, go to Step 13. If $[Tp]^k$ becomes nearly fixed as described in Appendix A and Sec. III.D, then the Markov chain converges and go to Step 14; otherwise, $s = s'$ and go to Step 2.

Step 13: If the probability of each scenario becomes nearly fixed, then go to Step 14; otherwise, $s = s'$ and go to Step 2.

Step 14: $IT = IT + 1$.

Step 15: If $IT = IT^{max}$(10000 herein), then compute LOLP/LOLE and stop; otherwise, $s = 1$ and go to Step 2.

In Step 15, the LOLP and LOLE can be calculated as follows.

$$\text{LOLP} = \frac{td}{TD} \tag{11}$$

$$\text{LOLE} = \text{LOLP} \times 8760(\text{hours/year}) \tag{12}$$

A flow chart showing the stages of the proposed method is provided in Fig. 2.

IV. SIMULATION RESULTS

A Python code was developed to integrate the PSS/E power flow software with the Taiwan power system data to study the reliability. A personal computer with Intel@ Core® i7-8700 CPU@ 4.60GHz, and 32.00GB RAM was used.

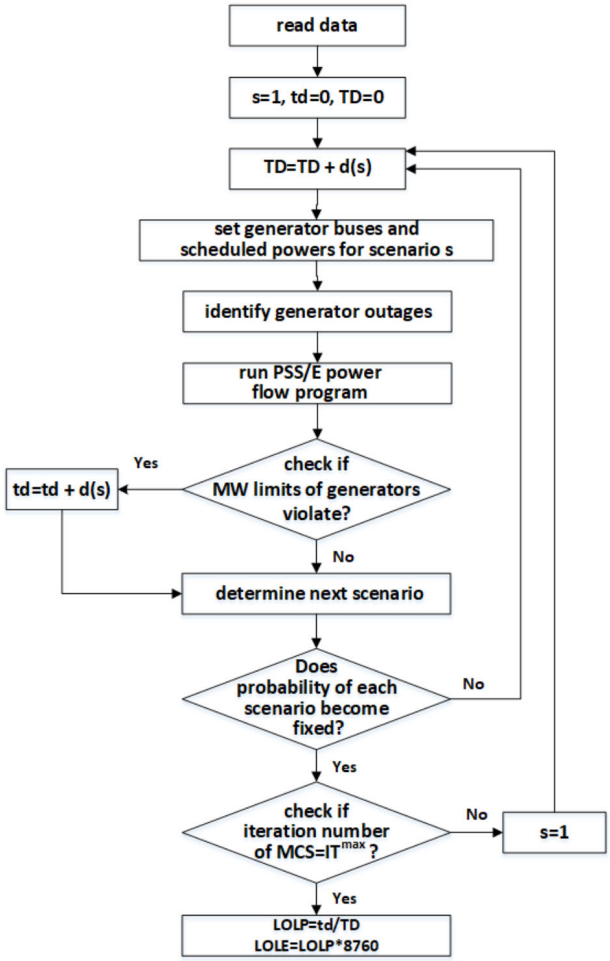

FIGURE 2. Flow chart showing stages of proposed method.

A. MARKOV STATES OF LOAD, PHOTOVOLTAIC POWER AND WIND POWER

The 8760 system loads were clustered into 15 states, as described in Sec. III.A. Table 2 shows these 15 states whose probabilities are within the range [0.03, 0.09] with durations from 1.46h to 3.59h. It is interesting to find that state 1 has the smallest probability but the longest duration. Please note that the values of powers shown in Table 2 are the vectors V_c (centers of clusters) in (7).

The 8760 irradiances in 2018 from NASA were input to the HOMER software to produce photovoltaic power values in the central area of Taiwan. The 8760 photovoltaic powers were clustered into 8 states, as described in Sec. III.A. As shown in Table 3, the probabilities of states (except state 1) are within the range [0.04, 0.10]. State 1 covers the evening, midnight and early morning with a large probability of 0.58 and a long duration of 13.79 h. Assume that the characteristics (probability and duration) in the northern and southern areas are the same as those of the central area. The ratio of power generations in the northern, central and southern areas is 1:53:33. Please note that the values of power shown in Table 3 are the vectors V_c (centers of clusters) in (7).

TABLE 2. Markov model of system loads.

State	Power (MW)	Probability	Duration (h)
1	20060.46	0.03	3.59
2	21726.07	0.05	2.33
3	23226.15	0.08	2.29
4	24520.35	0.09	1.79
5	25678.88	0.08	1.51
6	26726.74	0.09	1.53
7	27795.25	0.09	1.56
8	28847.09	0.08	1.49
9	29902.93	0.08	1.46
10	30888.40	0.08	1.60
11	32095.95	0.07	1.68
12	33239.37	0.06	1.74
13	34638.06	0.05	2.32
14	36245.59	0.04	1.74
15	37937.95	0.03	3.47

TABLE 3. Markov model of PV power generation in Central Taiwan.

State	Power (MW)	Probability	Duration (h)
1	20.345	0.58	13.79
2	1198.980	0.10	1.29
3	2345.018	0.08	1.53
4	3552.044	0.06	1.23
5	4815.925	0.05	1.32
6	6237.054	0.05	1.24
7	7767.298	0.04	1.42
8	9308.608	0.04	2.57

The 8760 historic wind speeds in the offshore wind farms in 2018 from the Center Weather Bureau in Taiwan were investigated. These wind speeds were also input to the HOMER software to produce wind power generation values of a wind turbine hub at a specific height. Table 4 shows the 13 Markov states of offshore wind farms. In state 13, the offshore wind farms produce 5326.93 MW with a high probability of 0.27 and a long duration of 4.21 h. Assume that the characteristics (probability and duration) of the offshore wind powers are the same as those of the onshore ones. The ratio of wind speeds in the offshore and onshore wind farms is 1.2:1. The powers shown in Table 4 are the vectors V_c (centers of clusters) in (7).

The corresponding transition probability matrics for Tables 2, 3 and 4 are provided in Appendix B.

The above results from Tables 2 through 4 were integrated to be 1560 scenarios of the Taiwan power system in 2025. Thus, the number of dimensions of both the transition probability matrix $[Tp]$ and the state transition matrix $[Ts]$ is 1560×1560. $[Tp]^k$ can converge with a tolerance of 10^{-4} (or 10^{-6}) when Markov chain index k is 63 (or 159). Fig. 3 illustrates the convergence pattern of iterations for $[Tp]^k$ if the tolerance is set to 10^{-4}. The y values in Fig. 2 denote the absolute value of the maximum element of $\left([Tp]^k - [Tp]^{k-1}\right)$.

B. VALIDATION OF PROPOSED METHOD

Validating the proposed method is the first step in ensuring that the proposed scenario-based reliability study is

TABLE 4. Markov model of offshore wind farms.

State	Power (MW)	Probability	Duration (h)
1	6.86	0.28	1.91
2	221.27	0.08	1.65
3	508.34	0.05	1.44
4	875.49	0.05	1.48
5	1298.81	0.04	1.27
6	1756.53	0.03	1.31
7	2220.71	0.03	1.27
8	2721.19	0.03	1.27
9	3221.95	0.02	1.25
10	3764.67	0.03	1.31
11	4274.70	0.03	1.39
12	4861.05	0.06	1.67
13	5326.93	0.27	4.21

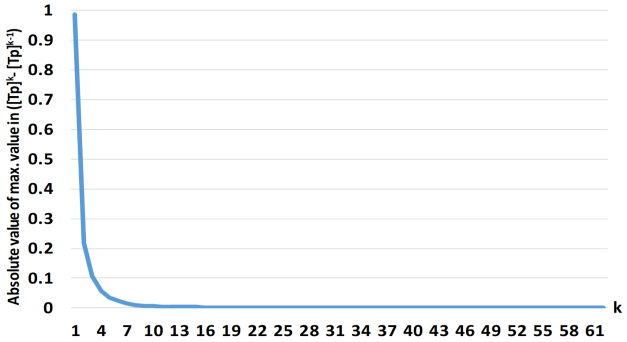

FIGURE 3. Convergence of transition probability matrix [*Tp*].

applicable. However, creating 1560 scenarios with the PSS/E data format by setting hourly loads at different buses and hourly power generations at various generators for the bulk Taiwan power system is almost impossible. Consequently, in this paper, one-week data (168 hours) rather than one-year data are used to validate the proposed method. The week with the summer peak load was considered: the loads are within [26.193, 39.718] GW; the maximum photovoltaic and wind powers in that week are estimated to be 15.516 and 6.028 GW, respectively.

In order to carry out a comparative study, the load, photovoltaic power and wind power are clustered into 6, 4 and 6 groups, respectively. Restated, 144 ($= 6 \times 4 \times 6$) scenarios, somewhat fewer than the 168 chronological cases, will be studied.

Two traditional MCSs, considering 168 chronological cases, were used for comparison: (a) only check the real power balance (method in [19]) and (b) run AC power flow studies (method in [14]). The method in [14] can be regarded as a benchmark method, which determines whether there are problems such as a shortage of generation capacity, overloading of the transmission lines or node voltage violation by conducting the AC power flow calculation. As shown in Table 5, the proposed method yields the same LOLP and LOLE as the method in [14]; however, the CPU time required by the proposed method is less than that required by the

TABLE 5. Validation of proposed method.

	LOLP	LOLE (hrs/y)	CPU time (s)
Method in [19]	0.00096	8.416	7.5
Method in [14]	0.00129	11.304	612.6
Proposed Method	0.00129	11.304	501.3

TABLE 6. Comparison of results among different load clusters.

	LOLP	LOLE (hrs/y)	CPU time (s)
9×8×13 scenarios	0.00046	4.029	509.1
15×8×13 scenarios	0.00122	10.687	523.6
25×8×13 scenarios	0.00115	10.074	542.4

TABLE 7. Comparison of results among different achieved renewable generation capacities.

Various Achieved Targets	LOLP	LOLE (hrs/y)	CPU time (s)
50% target	0.00206	18.045	543.3
75% target	0.00161	14.103	531.4
100% target	0.00122	10.687	523.6

method in [14]. Although the traditional method in [19] is the fastest, its obtained LOLP and LOLE are very different from those obtained by the method in [14]. The simulation results reveal that the traditional method in [19] is too optimistic.

C. COMPARISON OF RESULTS AMONG DIFFERENT NUMBERS OF SCENARIOS

The number of clusters associated with a time-series affect the accuracy of calculation of the LOLP/LOLE. Since the system load has the largest discrete size for clustering among three time series, various numbers of clusters of the load data were studied. In addition to 15 clusters, 9 and 25 load clusters were also explored herein; the numbers of clusters associated with photovoltaic (8) and wind (13) power generations are fixed. When the load data were clustered into 25 groups, 2600 scenarios have to be investigated, resulting in the longest CPU times, as shown in Table 6. The proposed $15 \times 8 \times 13$ scenarios yielded almost the same result as $25 \times 8 \times 13$ scenarios. When the load was clustered into 9 groups, $9 \times 8 \times 13$ scenarios yielded an optimistic result with a smaller LOLP and a shorter CPU time.

D. COMPARISON OF RESULTS ASSOCIATED WITH ACHIEVED RENEWABLE POWER CAPACITY TARGETS

The target capacities of photovoltaics and wind farms in 2025 are 20 GW and 6.938 GW, respectively. This subsection compares the LOLP/LOLE results that are obtained by assuming various ratios (50%, 75% and 100%) of these achieved capacities. Table 7 shows that the scenarios in which the target is reached have the highest reliability for the following reasons. When the achieved target is low, many combined cycle units must be on-line to meet the demand; however, the power generation capacity of a combined cycle unit is generally 200∼800 MW while those of photovoltaic units and wind farms are close to 100 MW. The inadequacy in a power system becomes severe when a forced outage occurs at a combined cycle unit.

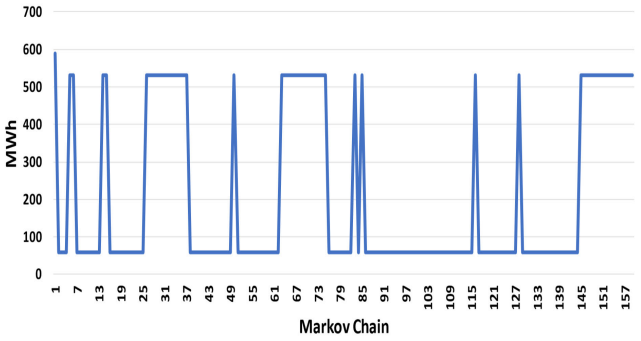

FIGURE 4. Variation of total MWh in a Markov chain (100% of renewables target met; 590 MW/MWh).

TABLE 8. Comparison of results among different achieved renewable power capacities with 590 MW BESS.

Various Achieved Targets	LOLP	LOLE (hrs/y)	CPU time (s)
50% target with BESS	0.00166	14.542	524.1
75% target with BESS	0.00143	12.527	517.5
100% target with BESS	0.00104	9.110	512.6

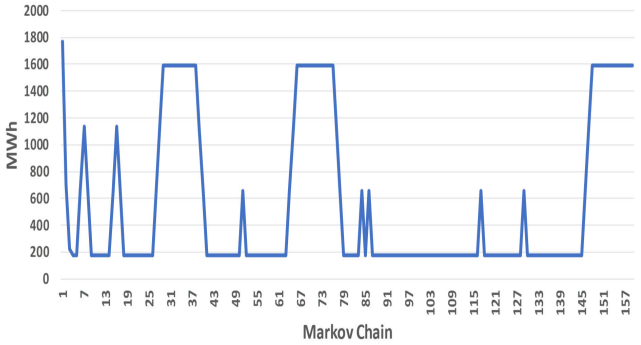

FIGURE 5. Variation of total MWh in a Markov chain (100% renewables target; 1770 MW/MWh).

Accordingly, small and distributed renewables may result in high reliability although the FOR (0.0500) of renewables is slightly larger than that (0.0414) of a combined cycle unit.

E. IMPACT OF BESS ON RELIABILITY

The reliability of the Taiwan power system was further studied by considering the BESS (590 MW and 590 MWh). The state-of-charge (SOC) was set within [10%, 90%] (59∼531MWh) [33]. Fig. 4 plots the variation of total MWh in a Markov chain, iterated from a scenario to another scenario until convergence, in one MCS. Table 8 shows the LOLP/LOLE that is obtained with a fixed BESS of 590 MW and 590 MWh. For a given achieved target of renewable generation capacity, the LOLE can be reduced if the BESS is allocated in the power system by comparing the results in Tables 7 and 8. The BESS with a fixed 590 MW/590 MWh can greatly improve the LOLE (from 18.045 to 14.542 hrs/year) with 50% of the renewable generation capacity target achieved.

TABLE 9. Comparison of results among different capacities/energies of BESS (100% of renewables target met).

BESS	LOLP	LOLE (hrs/y)	CPU time (s)
590MW/MWh	0.00104	9.110	512.6
1180MW/MWh	0.00098	8.585	517.4
1770MW/MWh	0.00096	8.409	516.8

The BESS of 590 MW is much smaller than the total renewable capacity. Thus, further simulations that consider 1180MW/1180MWh and 1770MW/1770MWh were carried out. Assume that the renewable capacity target is met. Fig 5 plots the variation of total MWh in a Markov chain for the 1770MW/1770MWh BESS in the MCS. Although the capacities/energies of the BESS were doubled or tripled, the decreases of the LOLE were rather limited, as shown in Table 9.

V. CONCLUSION

A novel scenario-based method is proposed for the analysis of power system reliability in this paper. The studied scenarios can be aggregated by Markov models of chronological loads, photovoltaic power generations and wind power generations. Full power flow studies, rather than a simple check on the real power balance, are carried out to assess the adequacy of the composite power system in terms of the LOLP and LOLE. This is especially essential for a large composite power system with a high penetration of renewables, in which the power generation resources are not allocated uniformly. The 2025 Taiwan power system with 2078 buses is used to demonstrate the applicability of the proposed method. The 1560×1560 probability transition matrix of this bulk power system can converge in a finite Markov chain. The computational time required for the proposed method is substantially reduced by considering scenarios rather than chronological cases in the Monte-Carlo simulation. A high penetration of renewables and energy storage systems can reduce the LOLP and LOLE. Future studies will consider the coordination of reliability and stability in a bulk power system with a high penetration of renewables.

APPENDIX A

This appendix provides the convergence theorem for a Markov chain. For a sequential time-series, the computation is straightforward from hour 1 to hour 8760. However, for the Markov states, state m can be moved to any other state in a manner that depends on the transition rates (probabilities), as in (4). Generally, an irreducible and aperiodic Markov chain can converge to a steady state [29].

Let the probability transition matrix $[Tp]$ of a two-state Markov model be $\begin{bmatrix} \alpha & 1-\beta \\ 1-\alpha & \beta \end{bmatrix}$ where α and β are within the range of (0,1). Then, the final two states will converge to a steady state as follows.

$$\lim_{k\to\infty} \frac{1}{2-\alpha-\beta} \begin{bmatrix} 1-\beta \\ 1-\alpha \end{bmatrix} \tag{A-1}$$

where k is the number of steps to move.

After the first iteration of the MCS, a steady-state $[Tp]$ is obtained. In the subsequent iterations of the MCS, this constant $[Tp]$ will be utilized to determine scenario $\mathbf{s}'$.

APPENDIX B

This appendix provides the corresponding transition probability matrices for the Markov models of system load, PV and wind, as shown in Tables 2, 3 and 4.

Below is the 15×15 transition probability matrix of the system load as shown at the bottom of this page.

Below is the 8×8 transition probability matrix of PV power:

$$\begin{bmatrix}
0.21 & 0.23 & 0.05 & 0.00 & 0.00 & 0.38 & 0.02 & 0.11 \\
0.21 & 0.25 & 0.01 & 0.00 & 0.00 & 0.08 & 0.14 & 0.24 \\
0.06 & 0.01 & 0.61 & 0.00 & 0.00 & 0.23 & 0.00 & 0.00 \\
0.00 & 0.05 & 0.00 & 0.23 & 0.06 & 0.00 & 0.25 & 0.27 \\
0.00 & 0.00 & 0.00 & 0.38 & 0.93 & 0.00 & 0.05 & 0.00 \\
0.25 & 0.10 & 0.33 & 0.00 & 0.00 & 0.30 & 0.00 & 0.01 \\
0.02 & 0.14 & 0.00 & 0.26 & 0.01 & 0.00 & 0.34 & 0.18 \\
0.25 & 0.22 & 0.00 & 0.13 & 0.00 & 0.01 & 0.20 & 0.19
\end{bmatrix}$$

$$\begin{bmatrix}
0.37 & 0.00 & 0.00 & 0.01 & 0.07 & 0.02 & 0.00 & 0.16 & 0.02 & 0.00 & 0.00 & 0.40 & 0.00 & 0.00 & 0.00 \\
0.00 & 0.42 & 0.00 & 0.00 & 0.20 & 0.00 & 0.00 & 0.00 & 0.00 & 0.00 & 0.22 & 0.00 & 0.00 & 0.00 & 0.00 \\
0.00 & 0.00 & 0.73 & 0.00 & 0.00 & 0.00 & 0.12 & 0.00 & 0.00 & 0.00 & 0.00 & 0.00 & 0.00 & 0.02 & 0.00 \\
0.07 & 0.00 & 0.00 & 0.36 & 0.00 & 0.16 & 0.00 & 0.02 & 0.00 & 0.36 & 0.00 & 0.04 & 0.02 & 0.00 & 0.01 \\
1.00 & 0.22 & 0.00 & 0.00 & 0.56 & 0.00 & 0.00 & 0.00 & 0.28 & 0.00 & 0.02 & 0.00 & 0.00 & 0.00 & 0.00 \\
1.03 & 0.00 & 0.00 & 0.36 & 0.00 & 0.32 & 0.00 & 0.06 & 0.02 & 0.02 & 0.00 & 0.14 & 0.02 & 0.00 & 0.00 \\
0.00 & 0.00 & 0.25 & 0.00 & 0.00 & 0.00 & 0.57 & 0.00 & 0.00 & 0.00 & 0.00 & 0.00 & 0.03 & 0.11 & 0.05 \\
1.31 & 0.02 & 0.00 & 0.00 & 0.03 & 0.01 & 0.00 & 0.39 & 0.18 & 0.00 & 0.00 & 0.02 & 0.00 & 0.00 & 0.00 \\
0.01 & 0.07 & 0.00 & 0.00 & 0.13 & 0.00 & 0.00 & 0.33 & 0.43 & 0.00 & 0.03 & 0.01 & 0.00 & 0.00 & 0.00 \\
0.02 & 0.00 & 0.00 & 0.16 & 0.00 & 0.02 & 0.00 & 0.00 & 0.00 & 0.36 & 0.00 & 0.07 & 0.39 & 0.01 & 0.03 \\
0.00 & 0.27 & 0.00 & 0.00 & 0.00 & 0.00 & 0.00 & 0.00 & 0.00 & 0.00 & 0.73 & 0.00 & 0.00 & 0.00 & 0.00 \\
0.19 & 0.00 & 0.00 & 0.02 & 0.01 & 0.38 & 0.00 & 0.04 & 0.07 & 0.01 & 0.00 & 0.30 & 0.00 & 0.00 & 0.00 \\
0.00 & 0.00 & 0.00 & 0.03 & 0.00 & 0.07 & 0.00 & 0.00 & 0.00 & 0.17 & 0.00 & 0.02 & 0.34 & 0.02 & 0.32 \\
0.00 & 0.00 & 0.02 & 0.00 & 0.00 & 0.00 & 0.27 & 0.00 & 0.00 & 0.05 & 0.00 & 0.00 & 0.03 & 0.56 & 0.15 \\
0.00 & 0.00 & 0.00 & 0.06 & 0.00 & 0.02 & 0.04 & 0.00 & 0.00 & 0.03 & 0.00 & 0.00 & 0.17 & 0.28 & 0.44
\end{bmatrix}$$

$$\begin{bmatrix}
0.46 & 0.01 & 0.00 & 0.03 & 0.00 & 0.02 & 0.01 & 0.13 & 0.20 & 0.00 & 0.04 & 0.02 & 0.01 \\
0.01 & 0.72 & 0.00 & 0.00 & 0.00 & 0.01 & 0.00 & 0.13 & 0.01 & 0.03 & 0.08 & 0.00 & 0.00 \\
0.00 & 0.00 & 0.33 & 0.00 & 0.12 & 0.01 & 0.06 & 0.00 & 0.00 & 0.18 & 0.04 & 0.01 & 0.03 \\
0.03 & 0.00 & 0.01 & 0.36 & 0.00 & 0.06 & 0.01 & 0.01 & 0.12 & 0.01 & 0.03 & 0.17 & 0.02 \\
0.00 & 0.00 & 0.24 & 0.01 & 0.43 & 0.01 & 0.03 & 0.00 & 0.01 & 0.07 & 0.11 & 0.01 & 0.03 \\
0.01 & 0.00 & 0.01 & 0.04 & 0.01 & 0.23 & 0.05 & 0.00 & 0.02 & 0.02 & 0.02 & 0.16 & 0.17 \\
0.00 & 0.00 & 0.05 & 0.00 & 0.02 & 0.08 & 0.28 & 0.00 & 0.00 & 0.14 & 0.03 & 0.02 & 0.14 \\
0.16 & 0.08 & 0.00 & 0.03 & 0.00 & 0.01 & 0.00 & 0.55 & 0.03 & 0.00 & 0.04 & 0.02 & 0.00 \\
0.14 & 0.00 & 0.00 & 0.20 & 0.00 & 0.01 & 0.01 & 0.02 & 0.34 & 0.00 & 0.02 & 0.06 & 0.02 \\
0.00 & 0.02 & 0.14 & 0.01 & 0.04 & 0.03 & 0.18 & 0.00 & 0.01 & 0.31 & 0.04 & 0.02 & 0.06 \\
0.17 & 0.17 & 0.19 & 0.15 & 0.37 & 0.18 & 0.17 & 0.16 & 0.19 & 0.19 & 0.51 & 0.15 & 0.18 \\
0.01 & 0.00 & 0.01 & 0.15 & 0.00 & 0.20 & 0.03 & 0.00 & 0.06 & 0.01 & 0.02 & 0.26 & 0.05 \\
0.01 & 0.00 & 0.02 & 0.02 & 0.01 & 0.15 & 0.17 & 0.00 & 0.01 & 0.04 & 0.02 & 0.10 & 0.29
\end{bmatrix}$$

Above is the 13×13 transition probability matrix of wind power as shown at the top of this page.

REFERENCES

[1] C. Vartanian, R. Bauer, L. Casey, C. Loutan, D. Narang, and V. Patel, "Ensuring system reliability," *IEEE Power Energy Mag.*, vol. 16, no. 6, pp. 52–63, Nov./Dec. 2018.

[2] P. H. Larsen, M. Lawson, K. H. LaCommare, and J. H. Eto, "Severe weather, utility spending, and the long-term reliability of the US power system," *Energy*, vol. 198, May 2020, Art. no. 117387.

[3] G. S. Seck, V. Krakowski, E. Assoumou, N. Maïzi, and V. Mazauric, "Embedding power system's reliability within a long-term energy system optimization model: Linking high renewable energy integration and future grid stability for France by 2050," *Appl. Energy*, vol. 257, Jan. 2020, Art. no. 114037.

[4] D. Min, J.-H. Ryu, and D. G. Choi, "Effects of the move towards renewables on the power system reliability and flexibility in South Korea," *Energy Rep.*, vol. 6, pp. 406–417, Nov. 2020.

[5] T. Lap, R. Benders, F. van der Hilst, and A. Faaij, "How does the interplay between resource availability, intersectoral competition and reliability affect a low-carbon power generation mix in Brazil for 2050?" *Energy*, vol. 195, Mar. 2020, Art. no. 116948.

[6] R. Billinton and R. N. Allan, "Power-system reliability in perspective," *IEE Electron. Power*, vol. 30, no. 3, pp. 231–236, Mar. 1984.

[7] A. M. Rei, A. M. L. da Silva, J. L. Jardim, and J. C. O. Mello, "Static and dynamic aspects in bulk power system reliability evaluations," *IEEE Trans. Power Syst.*, vol. 15, no. 1, pp. 189–195, Feb. 2000.

[8] R. Billinton and K. Chu, "Early evolution of LOLP: Evaluating generating capacity requirements," *IEEE Power Energy Mag.*, vol. 13, no. 4, pp. 88–98, Jul. 2015.

[9] S. A. Rashidaee, T. Amraee, and M. Fotuhi-Firuzabad, "A linear model for dynamic generation expansion planning considering loss of load probability," *IEEE Trans. Power Syst.*, vol. 33, no. 6, pp. 6924–6934, Nov. 2018.

[10] J. Choi, T. D. Mount, R. J. Thomas, and R. Billinton, "Probabilistic reliability criterion for planning transmission system expansions," *IEE Proc. Gener., Transmiss. Distrib.*, vol. 153, no. 6, pp. 719–727, Nov. 2006.

[11] M. Xu and X. Zhuan, "Optimal planning for wind power capacity in an electric power system," *Renew. Energy*, vol. 53, pp. 280–286, May 2013.

[12] V. Deulkar, J. Nair, and A. A. Kulkarni, "Sizing storage for reliable renewable integration: A large deviations approach," *J. Energy Storage*, vol. 30, Aug. 2020, Art. no. 101443.

[13] K. Xie, Y. Huang, B. Hu, H. Tai, L. Wang, and Q. Liao, "Reliability evaluation of bulk power systems using the uniform design technique," *IET Gener., Transmiss. Distrib.*, vol. 14, no. 3, pp. 400–407, Feb. 2020.

[14] L. Peng, B. Hu, K. Xie, H.-M. Tai, and K. Ashenayi, "Analytical model for fast reliability evaluation of composite generation and transmission system based on sequential Monte Carlo simulation," *Int. J. Electr. Power Energy Syst.*, vol. 109, pp. 548–557, Jul. 2019.

[15] J. Dong, F. Gao, X. Guan, Q. Zhai, and J. Wu, "Storage-reserve sizing with qualified reliability for connected high renewable penetration micro-grid," *IEEE Trans. Sustain. Energy*, vol. 7, no. 2, pp. 732–743, Apr. 2016.

[16] Y. Guo, S. Li, C. Li, and H. Peng, "Short-term reliability assessment for Islanded microgrid based on time-varying probability ordered tree screening algorithm," *IEEE Access*, vol. 7, pp. 37324–37333, 2019.

[17] X. Song, Y. Zhao, J. Zhou, and Z. Weng, "Reliability varying characteristics of PV-ESS-based standalone microgrid," *IEEE Access*, vol. 7, pp. 120872–120883, 2019.

[18] N. Y. Soltani and A. Nasiri, "Chance-constrained optimization of energy storage capacity for microgrids," *IEEE Trans. Smart Grid*, vol. 11, no. 4, pp. 2760–2770, Jul. 2020.

[19] R. Billinton and R. Karki, "Capacity expansion of small isolated power systems using PV and wind energy," *IEEE Trans. Power Syst.*, vol. 16, no. 4, pp. 892–897, Nov. 2001.

[20] S. S. Raghuwanshi and R. Arya, "Reliability evaluation of stand-alone hybrid photovoltaic energy system for rural healthcare centre," *Sustain. Energy Technol. Assessments*, vol. 37, Feb. 2020, Art. no. 100624.

[21] M. Theristis and I. A. Papazoglou, "Markovian reliability analysis of standalone photovoltaic systems incorporating repairs," *IEEE J. Photovolt.*, vol. 4, no. 1, pp. 414–422, Jan. 2014.

[22] J. Jurasz, B. Ceran, and A. Orłowska, "Component degradation in small-scale off-grid PV-battery systems operation in terms of reliability, environmental impact and economic performance," *Sustain. Energy Technol. Assessments*, vol. 38, Apr. 2020, Art. no. 100647.

[23] H. Hashemi-Dezaki, A.-M. Hariri, and M. A. Hejazi, "Impacts of load modeling on generalized analytical reliability assessment of smart grid under various penetration levels of wind/solar/non-renewable distributed generations," *Sustain. Energy, Grids Netw.*, vol. 20, Dec. 2019, Art. no. 100246.

[24] V. K. Prajapati and V. Mahajan, "Reliability assessment and congestion management of power system with energy storage system and uncertain renewable resources," *Energy*, vol. 215, Jan. 2021, Art. no. 119134.

[25] H. G. Kwag and J. O. Kim, "Reliability modeling of demand response considering uncertainty of customer behavior," *Appl. Energy*, vol. 122, pp. 24–33, Jun. 2014.

[26] A. J. Veldhuis, M. Leach, and A. Yang, "The impact of increased decentralised generation on the reliability of an existing electricity network," *Appl. Energy*, vol. 215, pp. 479–502, Apr. 2018.

[27] Y.-Y. Hong and J.-J. Wu, "Determination of transformer capacities in an industrial factory with intermittent loads," *IEEE Trans. Power Del.*, vol. 19, no. 3, pp. 1253–1258, Jul. 2004.

[28] T. Manco and A. Testa, "A Markovian approach to model power availability of a wind turbine," in *Proc. IEEE Lausanne Power Tech*, Jul. 2007, pp. 1256–1261.

[29] A. Klenke, *Convergence of Markov Chains*. London, U.K.: Springer, 2014.

[30] J. C. Bezdek, R. Ehrlich, and W. Full, "FCM: The fuzzy c-means clustering algorithm," *Comput. Geosci.*, vol. 10, nos. 2–3, pp. 191–203, Jan. 1984.

[31] HOMER Energy LLC. *Homer Pro User Manual*. Accessed: Apr. 29, 2019. [Online]. Available: https://www.homerenergy.com/products/pro/docs/latest/-index.html

[32] *PSS/E Version 33, User Manual*, Siemens, Munich, Germany, 2018.

[33] R. H. Byrne, T. A. Nguyen, D. A. Copp, B. R. Chalamala, and I. Gyuk, "Energy management and optimization methods for grid energy storage systems," *IEEE Access*, vol. 6, pp. 13231–13260, 2018.

YING-YI HONG (Senior Member, IEEE) received the B.S.E.E. degree from Chung Yuan Christian University (CYCU), Taiwan, in 1984, the M.S.E.E. degree from National Cheng Kung University (NCKU), Taiwan, in 1986, and the Ph.D. degree from the Department of E.E., National Tsing-Hua University (NTHU), Taiwan, in December 1990. Sponsored by the Ministry of Education of R.O.C., he conducted research at the Department of E.E., University of Washington, Seattle, from August 1989 to August 1990. Since 1991, he has been with CYCU. He was the Dean of the College of Electrical Engineering and Computer Science, CYCU, from 2006 to 2012. He was promoted to be a Distinguished Professor in 2012 due to his exceptional performance in research, leadership, teamwork, and international collaboration. From 2012 to 2018, he served as a Secretary General at CYCU. He is currently the Dean of research and development at CYCU. His areas of interests include power system analysis and AI applications. In 2006, he received the Outstanding Professor of Electrical Engineering Award from the Chinese Institute of Electrical Engineering (CIEE), Taiwan. He was the Chair of the IEEE PES Taipei Chapter, in 2001.

CHIN-I WU received the B.S.E.E. and M.S.E.E. degrees from CYCU, in 2018 and 2020, respectively. His areas of interests include power system analysis and renewable energy.

TZU-HSUN HSIAO received the B.S. degree from National Central University, Taiwan, in 2009, and the Ph.D. degree from the National Taiwan University of Science and Technology, in 2014. Since 2014, he has been with the Nuclear Energy Research Institute of Taiwan. His research interests include power reliability analysis and energy risk analysis.

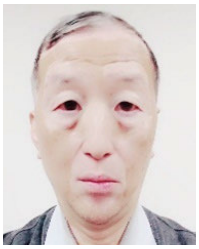

CHANG-SHIEN LIN received the Ph.D. degree from the Department of Electrical Engineering, National Taiwan University, Taiwan, in 2000. From 2000 to 2002, he was an Assistant Professor with the Nan-Kai University of Technology. From 2002 to 2009, he was an Assistant Professor with the Taipei City University of Technology. Since 2015, he has been a Technical Specialist with the Institute of Nuclear Energy Research of Taiwan. His research interests include power electronics, micro-grid systems, and AI for power systems.